Chemistry–A European Journal

Research Article
doi.org/10.1002/chem.202300394

Chemistry
Europe
European Chemical
Societies Publishing

www.chemeurj.org

Autonomous and Programmable Reorganization of DNA-Based Polymers Using Redox Chemistry**

Serena Gentile,[a] Erica Del Grosso,[a] Leonard J. Prins,[b] and Francesco Ricci*[a]

Abstract: We demonstrate here a strategy that allows the programmable and autonomous reorganization of self-assembled DNA polymers using redox chemistry. We have rationally designed different DNA monomers (tiles) that can co-assemble into tubular structures. The tiles can be orthogonally activated/deactivated with disulfide-linked DNA fuel strands that are degraded over time upon reduction because of the presence of a reducing agent in the system. The concentration of the disulfide fuels determines the activation kinetics of each DNA tile, which controls the degree of order/disorder in the formed co-polymer. The disulfide-reduction pathway can be employed together with enzymatic fuel-degradation pathways providing an additional level of control in the re-organization of DNA structures. Taking advantage of the different pH-sensitivities of disulfide-thiol and enzymatic reactions, we show that we can control the order in DNA-based co-polymers as a function of pH.

Introduction

A strong current interest in the field of supramolecular chemistry is aimed at creating sophisticated mechanisms to develop synthetic materials and polymers that, like their naturally-occurring counterparts, have the ability to re-organize and adapt in response to different molecular cues and can thus find applications in drug-delivery, sensing and diagnostics.[1–6] Promising strategies to create similar nature-inspired materials include the use of supramolecular co-polymers formed by two or more monomers each responding to a different input.[7,8] These multicomponent polymers can dynamically rearrange using different mechanisms and adapt in response to different molecular cues leading to structures with variable monomer distribution that can ultimately give different functionalities.[9–11] Significant advances in recent years have enabled the synthesis of similar multicomponent co-polymers with tunable composition and distribution of their constitutive units through elegant strategies like living crystallization-driven self-assembly,[12,13] seeded supramolecular polymerization[14–16] and fuel-driven reactions.[17–21] Despite the progress made in this direction, the ability to dynamically rearrange and reconfigure co-polymer structures in a highly programmable manner remains challenging mainly due to the lack of molecular programmability of the building blocks employed.

Synthetic DNA has recently emerged as a powerful material to engineer and reconfigure artificial supramolecular systems whose self-assembly can be finely controlled.[22–25] The high programmability and predictability of nucleic acid hybridization, in fact, allow to precisely assemble functional supramolecular structures and polymers. By coupling these systems with DNA-recognizing enzymes (nucleases, nickases, ligases etc) that are able to inactivate DNA fuel strands used as chemical triggers, it is also possible to introduce temporal control in synthetic devices and self-assembly processes and allow autonomous and controlled reconfiguration.[26–31] These examples clearly demonstrate the advantages of using synthetic DNA to create adaptable and reconfigurable synthetic materials. The use of enzymatic reactions to achieve this goal, however, is not without limitations: enzyme activity can be affected by the formed waste products and enzymes can have limited operational stability. Demonstrating the reconfiguration of DNA-based materials and the control over the distribution and organization of DNA-based polymers using non-enzymatic chemical reactions can provide an important stimulus to this field. Motivated by the above considerations, we propose here to use disulfide reduction as a way to reversibly and autonomously reconfigure DNA-based synthetic assemblies. We show that this non-enzymatic reaction is finely programmable, can be further controlled by external stimuli (i.e., pH) and can be also used in conjunction with enzyme-regulated reactions in the same system. The possibility of using additional regulatory mechanisms enables a higher degree of control over the chemically-fuelled reconfiguration of DNA-based assemblies.

[a] S. Gentile, Dr. E. Del Grosso, Prof. F. Ricci
     Department of Chemical Sciences and Technologies
     University of Rome Tor Vergata
     Via della Ricerca Scientifica, 00133 Rome (Italy)
     E-mail: francesco.ricci@uniroma2.it

[b] Prof. L. J. Prins
     Department of Chemical Sciences
     University of Padua
     Via Marzolo 1, 35131 Padua (Italy)

Results and Discussion

To demonstrate programmable and autonomous reorganization of nucleic acid assemblies (i.e., polymers) using redox chemistry, we have employed as model system DNA nanotubes, DNA-based structures that self-assemble through the non-covalent and isothermal inteactions of specifically designed DNA tiles.[26,32–35] These DNA tiles are formed through the interaction of five distinct DNA strands and contain four sticky ends (5-nt each) that allow spontaneous self-assembly into tubular structures with a mean diameter of 13.5 nm and an average persistence length of 4 μm (Figure S1).[26,34] The DNA tiles also contain a specific overhang single-stranded binding domain of 7-nt to which a 14-nt fuel strand can bind to invade one of the four sticky ends and induce the disassembly of the DNA structure (Figure S2).[26,31,36] It is possible to program different tiles to have the same sticky ends, so that they can co-assemble into the same tubular structure (from here defined as co-polymer). Each tile can also display a specific single-stranded DNA "tail" that can serve as orthogonal controller domain to which different complementary fuel strands can bind and invade one of the tile's sticky ends inducing the tile inactivation (and thus structure disassembly).[22,31] Each DNA tile can also be labeled with a different fluorophore (Cy3 for Red, R, tile and Cy5 for Green, G, tile) to independently monitor their distribution in the assembled co-polymer.

To achieve redox control over the autonomous reconfiguration of these DNA co-polymers we have employed DNA fuel strands that can be inactivated upon reduction.[23,37] To do that

we have split the DNA fuel strand into two halves and linked them with a disulfide bond. Such disulfide-linked fuels maintain the ability to invade and induce tile inactivation (and thus disassemble the structure). Upon reduction, however, the two split portions of the fuel will de-hybridize from their complementary fuel-binding domain allowing the spontaneous reactivation of the DNA tiles and the re-assembly of the DNA structures (Figures 1a, S3). The relative rate of activation and re-assembly of each tile (v_R and v_G for red and green tile, respectively) determines the tiles distribution in the co-polymer (Figure 1b).

Initially, we studied the kinetics of the re-assembly process for the red tiles alone at different concentrations of disulfide fuel strand and in the presence of a fixed concentration of the reducing agent (TCEP) (Figure 2a–d). The addition of the disulfide fuel causes the rapid disassembly of the structures followed by a gradual re-assembly induced by fuel reduction (Figures 2b and c, S4 and S5). We observe that the rate of re-assembly decreases from 0.37 ± 0.04 to 0.04 ± 0.01 assembled tiles/h upon increasing the disulfide fuel concentration from 1.5 to 10 μM (Figure 2d). Qualitative simulations using a kinetic model that contains the key equilibria and chemical reactions occurring in the system show that the re-activation rate of the self-assembly process (Figure 2c) cannot be simply explained by a slow reduction of the fuel in the system (see Supporting Information for more details on the simulation, Figures S6 and S7). Rather, the experimental observations are consistent with a model in which also the dissociation of the tile-waste complex is of kinetic relevance. High fuel concentrations lead to an
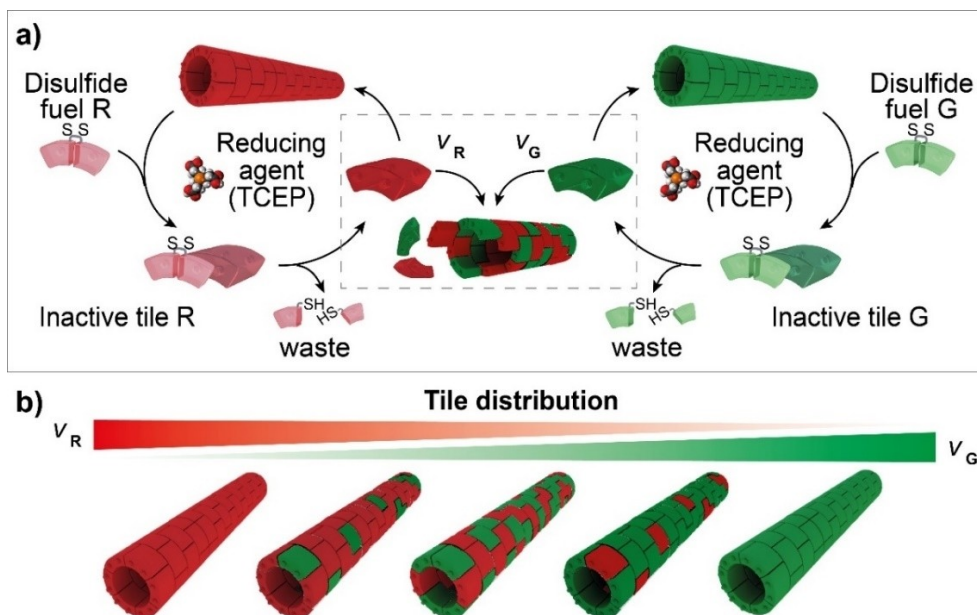

Figure 1. Disulfide-linked fuels to control DNA-tile distribution and DNA-based structures reorganization. a) The scheme shows a simplified cartoon of the self-assembly process. The DNA tiles are depicted as Lego brick with two holes and two knobs representing the 4 sticky ends responsible for self-assembly. The tiles are conjugated with two different fluorophores (Cy3 for red tiles, R and Cy5 for green tiles, G). The tiles share the same sticky ends and thus can co-assemble into a co-polymer structure. Each tile can be specifically inactivated by a disulfide-linked DNA strand (fuel R, fuel G). In a reducing environment (TCEP in solution) the disulfide fuel is reduced over time into two halves which de-hybridize from the tiles and lead to their re-activation and assembly into co-polymeric structures. See Figures S1–S3 for a more detailed visualization of the assembly/disassembly process. b) Tile distribution in the co-polymer can be controlled by the relative kinetics with which the two tiles are reactivated upon fuel degradation (v_R, v_G).
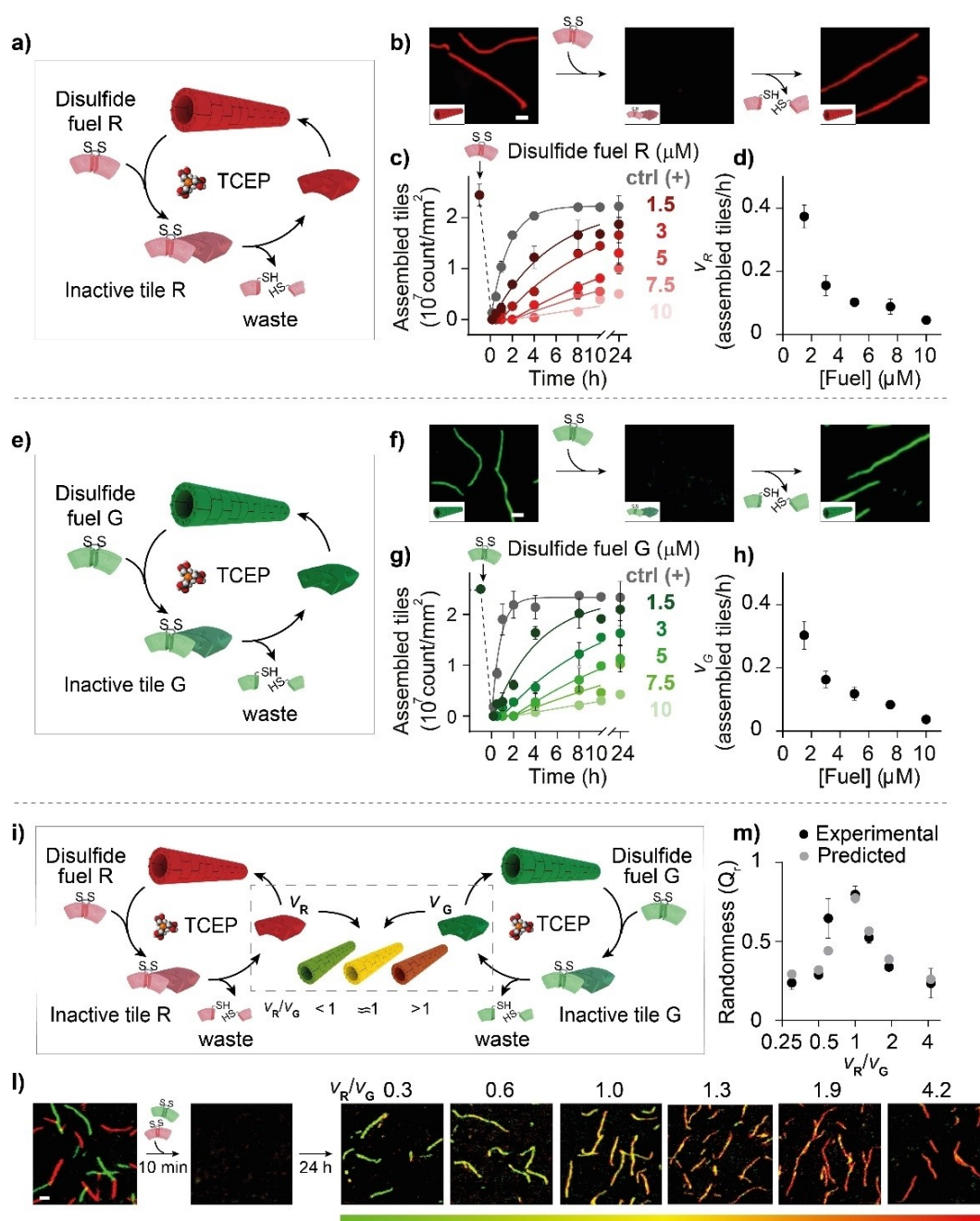
Figure 2. Programmable co-polymer tile distribution using redox reactions. a) Scheme of transient disassembly driven by a redox reaction for red tiles. The disulfide fuel (light red) binds the fuel-binding domain inducing the disassembly of the DNA-based homo-polymer structure. A reducing agent (here TCEP) acts as fuel-consuming unit reducing the fuel in two halves that spontaneously de-hybridize from the DNA tile. The reactivated tiles can then re-assemble into DNA-based red homo-polymers. b) Fluorescence microscopy images showing a representative experiment of transient disassembly. c) Transient disassembly of red homo-polymers at different concentrations of red disulfide fuels. d) Re-assembly rates (assembled tiles/h, calculated by linear fitting of the initial part of the kinetic curves in panel c) at different concentrations of red disulfide fuels. e–h) Transient disassembly driven by a redox reaction for green tiles. i) Scheme of structural reorganization from red and green homo-polymers to R/G co-polymers. Different distribution of the two tiles in the co-polymer can be achieved by modulating the v_R/v_G ratio. l) Fluorescence confocal images showing the reorganization into different R/G co-polymers at 24 h obtained at different v_R/v_G ratios (indicated). m) Plot of Q_r (randomness parameter) vs. v_R/v_G ratio. Black circles represent experimental data while the grey circles represent the predicted values obtained from the kinetic experiments of individual systems (see Supporting Information for more details on the prediction). [tile R] = [tile G] = 0.15 μM, [TCEP] = 300 μM, 1×TAE buffer + 12.5 mM MgCl$_2$, pH 8.0, 25 °C. Confocal images scale bar: 2.5 μm. Error bars represent standard deviation based on triplicate measurements.

increased population of the tile-waste duplex, which implies that a longer time is required to complete the assembly process. A virtually identical disulfide fuel-dependent behaviour

was also observed for green tiles leading to the re-assembly of green homo structures with rates (v_G) comparable to those of red tiles (Figures 2e–h, S8). Statistical analysis of length

Chemistry–A European Journal

Research Article
doi.org/10.1002/chem.202300394

Chemistry
Europe

European Chemical
Societies Publishing

distributions for red and green tiles are shown in Figures S5 and S9.

Using the above-determined re-assembly rates of disulfide-induced transient DNA re-assembly we can achieve the spontaneous reorganization of homo-polymers in a co-polymer with a predictable distribution of the two tiles (Figure 2i–m). To demonstrate this, we employed a solution containing two separate homo-polymers each formed by a single tile (red, R or green, G) which remain stable in the presence of the reducing agent (TCEP, 0.3 mM) (Figure S10). By varying the concentration of the two fuels we can achieve v_R/v_G values that span two orders of magnitude (i.e., from 0.3 to 4.2 assembled tiles/h, Figure 2l). By doing so we can obtain DNA co-polymers mostly formed by green tiles (when $v_R/v_G < 1$), by red tiles (when $v_R/v_G > 1$) or containing a statistical distribution of red and green tiles (when $v_R/v_G = 1$). To estimate the different tile distribution in the co-polymer we introduce here a randomness parameter (Q_r), inspired by other similar parameters,[38–40] that is obtained by dividing the number of co-localized assembled tiles (RG) for the number of total (co-localized + non-colocalized) assembled tiles (RG + R + G) at 24 h (Figure 2m, black circles, see Supporting Information for more details on the Q_r calculation). A Q_r of 1 would indicate a perfect randomness of the formed structures and a $Q_r < 1$ would indicate a lower randomness. As expected, the randomness values we obtain follow a bell-shaped trend with a maximum value ($Q_r = 0.80 \pm 0.05$) obtained when $v_R/v_G = 1.0$ and lower values when the rate of re-assembly of one of the two tiles is higher (Figure 2m, black circles). To demonstrate the programmability of the disulfide reduction we have predicted the randomness degree of the final co-polymer using the experimental data obtained with the two individual systems at different re-assembly rates (Figure 2a–h, see Supporting Information for more details on the Q_r prediction). By doing this we obtain values of Q_r that agree very well with the experimental data (Figure 2m, grey circles).

Because the fuel reduction generates a very predictable degradation product (i.e., the two reduced thiol oligonucleotides) it is also possible to control the kinetics of fuel dehybridization and thus the distribution of the two tiles in the co-polymer by rationally designing disulfide fuels with different lengths of the two portions (i.e., longer reduced fuel portions lead to a slower rate of de-hybridization) (Figure S11).

Redox-controlled DNA tile activation is also reversible. After fuel reduction is completed, an aliquot of oxidizing agent (NaBO₃) can be added to recreate the functional fuel. By doing so we observe disassembly of the polymers upon addition of the oxidixing agent, a result that supports the successful formation of the disulfide fuel (Figure S12).

Redox-controlled DNA tile activation can also tolerate extreme working conditions, contrarily to what happens with enzymatic reactions that have been previously exploited for the same purpose.[29–31] To demonstrate this, we performed redox-controlled transient disassembly after incubating the fuel consuming unit at temperatures comprised between 60 and 100 °C and observed no significant differences in efficiency with the experiments in which TCEP was stored at RT. As a comparison, the same experiment carried out with the

enzymatic reaction (i.e., using RNA as the fuel and RNase H as the fuel degrading unit) showed a progressively reduced efficiency above 60 °C (Figure S13).

The versatility of redox-controlled DNA tile reorganization is further demonstrated by employing in the same solution two non-interacting tile systems each labeled with a different fluorophore (Cy3, R and Cy5, G) and each containing a specific addressable fuel-binding domain (Figure 3a). The first system is represented by red inactive tiles bound to a disulfide red fuel similar to the systems described above (Figure 3b). In this case, reduction of the disulfide fuel leads to red tiles activation and assembly of red homo-polymers. For the second system we employed already formed green homo-polymers to which we added a duplex complex formed between the green fuel and a complementary disulfide strand. In this system the green fuel is inactive and can induce disassembly of the green homo-polymers only upon reduction of the disulfide complementary strand (Figure 3c). When these systems are combined, the addition of reducing agent (TCEP) causes an opposite effect on the red and green tiles. Reduction of the disulfide bonds results in an activation of the green fuel leading to disassembly of the green homo-polymers, but, at the same time, the red tiles are activated for self-assembly. Consequently, in time the system transits spontaneously from green to red homo-polymers (Figure 3d and e).

Interestingly, the above transition can be halted at will by altering the pH of the solution because the rate of disulfide reduction is almost brought to a stand at acidic pHs[41] (Figure 3f and g). We first confirmed that this pH-dependence is a result of the disulfide reduction by observing that no change in tile reactivation rate was achieved when a control DNA activator that removes the fuel from tiles through a strand displacement reaction was added at pH 8.0 and 6.0 (Figure S14). We thus performed the same reconfiguration from red to green homo-polymers shown above and, upon changing the pH of the solution from pH 8.0 to 6.0 after 2 h from the addition of the reducing agent, we stopped the structural re-organization. This is demonstrated by the constant values of assembled green and red structures (Figure 3f and g). By increasing again the pH of the solution to the original value (i.e., pH 8.0) the reconfiguration continues until completion (disassembly of green structures and assembly of red structures) (Figure 3f and g).

We argued that we could bring the control over reorganization of the system to an even higher level by including a second alternative fuel consuming-pathway. Indeed, the experimental conditions of the disulfide-reduction reaction we used here to control the assembly/disassembly of DNA polymers are compatible with enzymatic reaction.[29–31] This makes it in principle possible to control the reconfiguration of DNA structures using two fuel-consuming reactions (enzymatic and redox reactions). Motivated by this possibility we have thus employed one of the DNA tiles described above that is controlled by the disulfide redox reaction together with a different DNA tile controlled by an RNA fuel and an enzyme (RNase H) as fuel consuming unit.[31] The RNase H selectively hydrolyzes the RNA fuel when it is bound to the complementary DNA fuel-binding domain leading to the reactivation of the
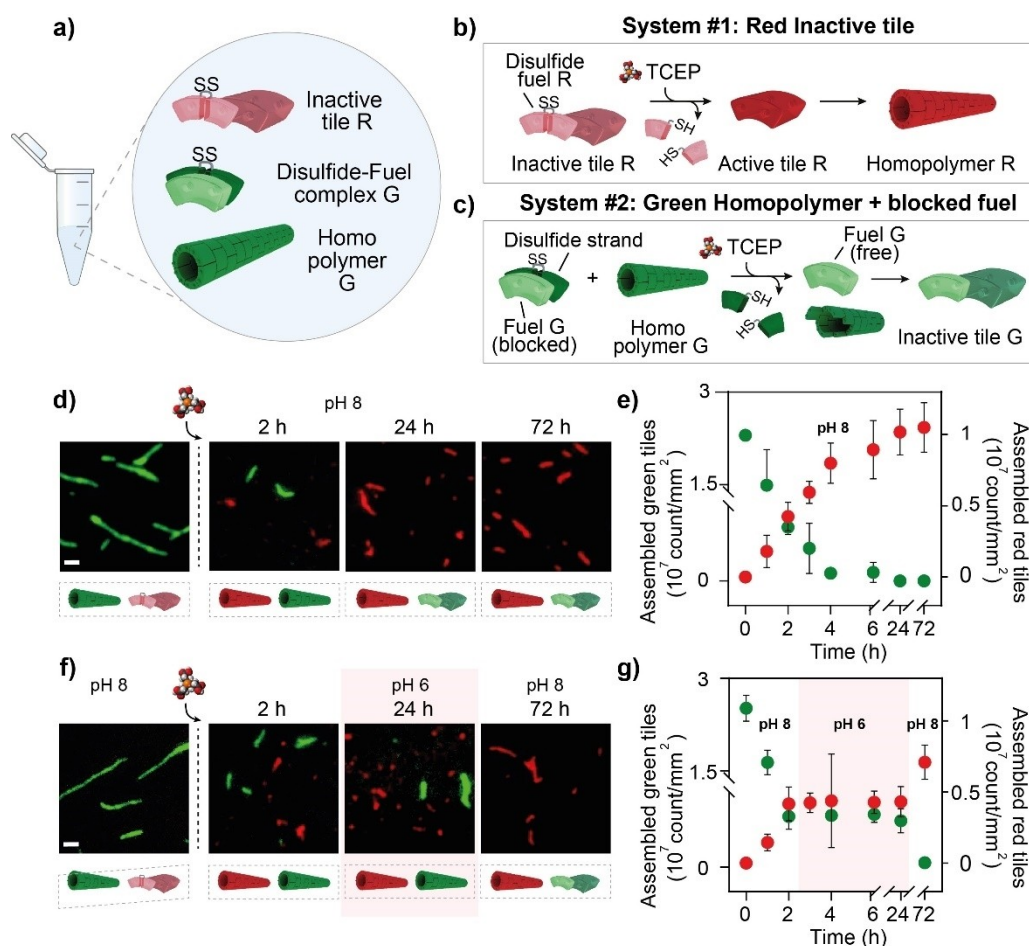
Figure 3. Dynamic assembly and disassembly of DNA polymers triggered by the addition of reducing agent (TCEP). a) DNA elements employed in this experiment. b) System #1: red inactive tiles bound to disulfide red fuel. Reduction of the disulfide fuel leads to tile activation and assembly of red homo-polymers. c) System #2: green homo-polymers together with green fuel bound to a complementary disulfide strand. Reduction of the disulfide strand leads to fuel release and disassembly of green homo-polymers. d) Fluorescence microscopy images showing the dynamic assembly (R) and disassembly (G) upon the reduction of both disulfide strands at pH 8.0 following the addition of reducing agent (TCEP). e) Plot of assembled red (R) and green (G) tiles vs. time after TCEP addition. f) Fluorescence microscopy images showing the dynamic assembly (R) and disassembly (G) when the pH solution changed from pH 8.0 to pH 6.0 and back to pH 8.0. g) Plot of assembled red (R) and green (G) tiles vs. time after TCEP addition. The red window represents the period in which the system is kept at pH 6.0. Scale bar: 1.5 μm. Error bars represent standard deviation based on triplicate measurements. [tile R] = 0.5 μM, [tile G] = 0.2 μM, [Disulfide fuel R] = 1 μM, [Disulfide complementary strand G] = [Fuel G] = 0.4 μM, [TCEP] = 3 mM, 1×TAE buffer + 12.5 mM MgCl₂, 25 °C.

DNA tiles and re-assembly into a polymeric structure. We first followed via fluorescent microscopy the re-assembly kinetics of each tile alone controlled by its specific mechanism at different concentrations of the two fuels (disulfide and RNA) and derived the values of the relative re-assembly rates ($v_{R\_disulfide}$, v_{G_enzyme}) (Figures S15 and S16).

Also in this case, by varying the re-assembly rates of the two systems (by changing the corresponding fuel concentration) we can obtain different types of DNA co-polymers (Figures 4a–d, S17). For example, using conditions in which the RNase H induced degradation (v_{G_enzyme}) is much faster than the disulfide reduction ($v_{R\_disulfide}$), we achieve the formation of block polymers (GR, GRG) which display long green sequences connected to smaller red portions (Figure 4b). Co-polymers with a similar distribution but with a predominant red part could be achieved for $v_{R\_disulfide}/v_{G\_enzyme} \gg 1$, implying that the enzymatic degradation is much slower than the disulfide reduction (Fig-

ure 4d). On the contrary, when $v_{R\_disulfide}/v_{G\_enzyme} \approx 1$, both tiles are reactivated with similar rates and co-assemble into structures with a random tile distribution takes place (Figure 4c). Statistical analysis of the confocal images in terms of average length ($<L>$) of green (G channel), red (R channel) and random (merged, M channel) structures supports the reconfiguration pathways achieved at different re-assembly rates of the two tiles (Figure 4e).

Finally, the use of two different fuel-consuming pathways (redox and enzymatic) offers the possibility to finely control co-polymer reorganization using pH as an external stimulus (Figure 5a). In fact, we have shown above that the disulfide reduction – reaction is highly sensitive to pH (they are extremely slow at acidic pHs and become more efficient at basic pHs) (Figure S18).[41] As a result, tile activation (red tiles) through disulfide fuel reduction is quite rapid at pH values above 8.0 and becomes extremely slow below pH 7.6 (Figur-
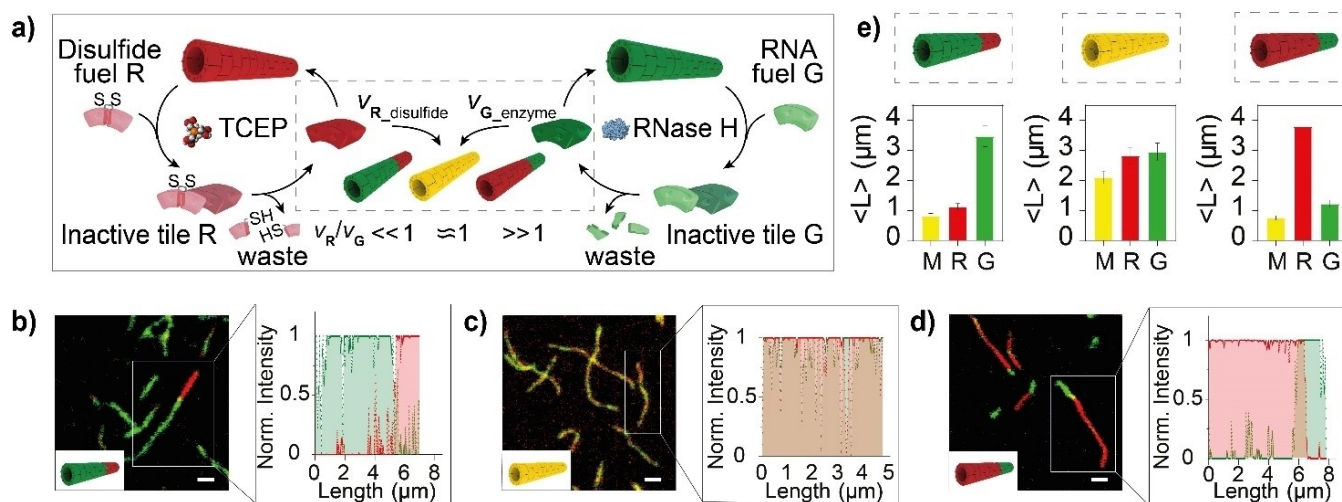
Chemistry–A European Journal

Research Article
doi.org/10.1002/chem.202300394

**Chemistry
Europe**
European Chemical
Societies Publishing

Figure 4. Programmable co-polymer tile reorganization using redox and enzymatic reactions. a) Scheme of spontaneous reorganization from red and green homo-polymers to R/G co-polymers upon the addition of different concentrations of the two fuels (disulfide, R and RNA, G). b–d) Fluorescence confocal images showing the reorganization into block co-polymers or statistical random co-polymers at 24 h obtained in presence of reducing agent (here TCEP) and RNase H. Analysis of a single block structure showing normalized pixel intensity of the green and red channels calculated over 0.5 μm segments along the line-profile. e) Statistical analysis of the average length of the final structures obtained at 24 h for each channel (red, R, green, G, and random, merged, M). [tile R] = [tile G] = 0.15 μM, [TCEP] = 3 mM, [Rnase H] = 30 U/mL, 1×TAE buffer + 12.5 mM MgCl$_2$, pH 8.0, 25 °C. Confocal images scale bar: 2.5 μm. Error bars represent standard deviation based on triplicate measurements.
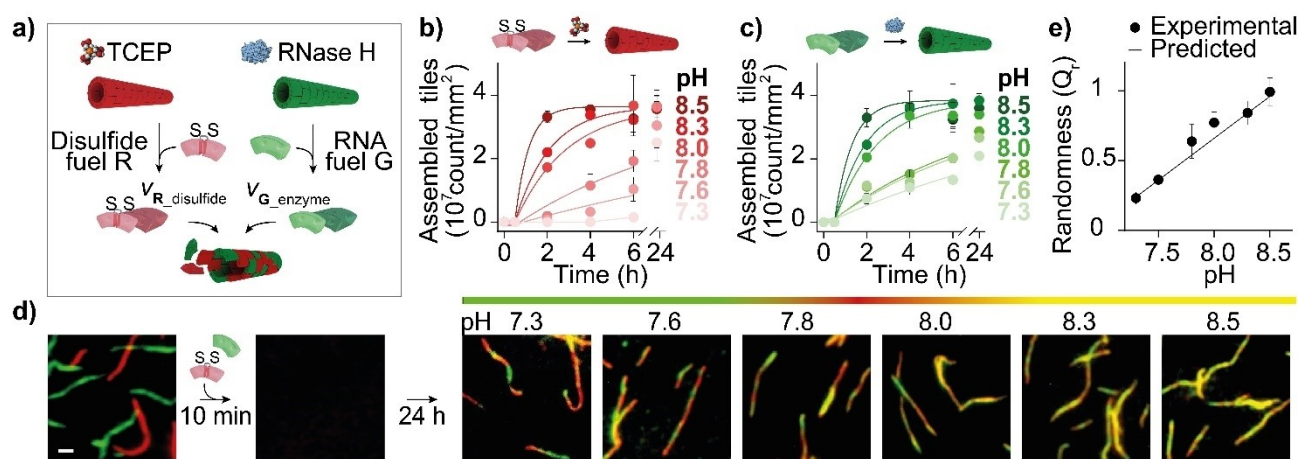

Figure 5. Programmable co-polymer tile distribution combining redox and enzymatic reactions and using pH as an external stimulus. a) Scheme of co-polymer reorganization driven by two different fuel-consuming pathways (redox and enzymatic). b) Re-assembly kinetics of red tiles into red homo-polymers at different pHs following reduction of disulfide fuel by TCEP. c) Re-assembly kinetics of green tiles into green homo-polymers at different pHs following RNA fuel degradation by RNase H. d) Fluorescence confocal images taken after fuel addition at different pHs. e) Plot of Q_r (randomness parameter) vs. pH. Circles represent experimental data while the solid line represents the predicted values obtained from the kinetic experiments of individual systems (panels b and c). [tile R] = [tile G] = 0.15 μM, [disulfide fuel R] = [RNA fuel G] = 1.5 μM, [TCEP] = 3 mM, [Rnase H] = 50 U/mL, 1×TAE buffer + 12.5 mM MgCl$_2$, 25 °C. Fluorescence microscopy images scale bar: 1.5 μm. Error bars represent standard deviation based on triplicate measurements.

es 5b, S18 and S19). RNase H activity is also pH-dependent but with a much less steeper dependency. When using RNA fuel and RNase H induced tile re-activation we thus observe only a slightly slower polymer re-assembly at pH below 7.6 compared to the same experiment carried out at pH above 8.0 (Figures 5c, S20).

Co-polymer re-organization achieved by adding disulfide and RNA fuels to a solution containing the two homo-polymers and the two fuel-consuming units (TCEP and RNase H) would thus provide different tiles distribution if performed under different pH conditions (Figure 5d). To quantify the different tile distribution achieved at different pHs we computed the randomness parameter (Q_r). As expected, after the addition of the two fuels the two homo-polymers are rapidly disassembled and then reassemble into co-polymers at different pH-dependent kinetics. At pH 8.5 the kinetics of tile reactivation is rapid for both fuels and thus we observe almost perfect random co-polymers with statistical distribution of the two tiles ($Q_r = 1.00 \pm 0.05$, Figure 5d and e). When performing the same experiment at lower pHs we observe a gradual transition from random to

Chem. Eur. J. **2023**, *29*, e202300394 (6 of 9)

© 2023 Wiley-VCH GmbH

more ordered co-polymers ($Q_r = 0.23 \pm 0.04$, at pH 7.3) (Figure 5d and e). The prediction of the composition calculated using the kinetics of each system at each pH tested (Figure 5b and c, see Supporting Information for more details on the Q_r prediction) correlate very well with the experimental data (Figure 5e, solid line vs. circles) providing further support to the hypothesis that redox and enzymatic reactions are highly programmable and easily tunable.

We finally set up an application in order to demonstrate a practical utility of the redox-controlled fuel degradation described here. More specifically, we employed our disulfide reduction pathway to achieve the transient visualization of DNA-based polymers. To do this, we have re-engineered a DNA tile displaying a single-stranded overhang (30-nt). The DNA tile can self-assemble into a DNA tubular structure but cannot be observed with a fluorescent microscope because it lacks the fluorescent label. We have then designed a duplex formed by a disulfide strand and a DNA complementary strand end-labeled with a fluorescent tag (Quasar570 fluorophore). This duplex also presents a single-strand domain complementary to the overhang of the tubular structure. The hybridization of this fluorophore-labeled disulfide duplex to the overhang strand makes it possible to visualize the DNA polymers (Figure S21a and b). In the presence of TCEP this visualization is transient because the labeled disulfide strand is degraded over time leading to the dehybridization of the fluorophore-labeled strand from the DNA tile. Such transient visualization remains efficient over 3 different reaction cycles (Figure S21c). As expected, a control experiments using a fluorophore-labeled strand of the same length but lacking the disulfide bond showed permanent (non-transient) visualization of the structure (Figure S21, red curve).

Conclusion

The strategy we present here provides control over the reorganization of DNA-based polymers exploiting redox reactions. To do this we rely on the use of disulfide-linked DNA fuels that can orthogonally activate/deactivate different DNA tiles that co-assemble into polymeric tubular structures. The effect exerted by the disulfide fuels is transient because of their gradual conversion into thiolated waste strands with low affinity. By controlling the residence time of the fuel in the system (initial concentration, pH-dependent reaction rate), we can regulate the kinetics of tile activation/deactivation and, consequently, the degree of order/disorder in the formed DNA polymers.

The use of a purely chemical pathway for fuel degradation presents several advantages compared to the most commonly used enzymatic reactions. First, the fuel degradation reaction is less affected by stability issues that can limit the use of enzymes. We demonstrate this by showing that disulfide redox reactions are well tolerated at temperatures that usually lead to complete inactivation of enzymes. Second, the redox reaction employed here is not affected by waste products (reduced thiol DNA strands) as often occurs with enzymatic reactions in which the formation of high concentration of product often limits the activity of the enzyme. Third, contrarily to enzymatic reactions, reduced thiols can be easily reoxidized making our approach fully reversible. Finally, the strategy we propose here is highly programmable: we can rationally design disulfide fuels with different lengths so that we can control in a precise way their dehybridization rate from the tiles. This, ultimately, allows to precisely control the rate of tiles re-activation.

Within the field of Dissipative DNA Nanotechnology, which regards DNA-based devices and structures that are driven by chemical fuel-to-waste conversion,[42] the availability of new synthetic fuel-consumption pathways permits an increase in the chemical space that can be explored by DNA-based systems. The availability of orthogonal reaction sets facilitates the emergence of complex DNA-based circuitries able to compute a large variety of complex operations. Several possible applications of the herein reported strategy can be envisioned. For example, 2D and 3D DNA-based structures and origami have been demonstrated useful in applications including drug delivery, sensing and bioimaging.[43–47] These assemblies are often used as molecular scaffolds to display different elements (recognition tags, biomolecules and optical labels) that provide specific functions.[48–51] The redox-controlled reorganization strategy we reported here could be used to control the distribution, organization and density of the functional decorative elements on such molecular scaffolds thus ultimately providing a tool to temporally control their function in a programmable fashion.

Experimental Section

Chemicals: Reagent-grade chemicals (DEPC-treated water, Na_2HPO_4, Trizma hydrochloride, Trizma base, Acetic acid, EDTA, Tris(2-carboxyethyl)phosphine (TCEP), KCl, $MgCl_2$, 1,4-Dithiothreitol (DTT)) were purchased from Sigma-Aldrich (St. Louis, Missouri, USA) and used without further purifications.

Enzyme: RNase H recombinant was purchased from New England BioLabs and stored at $-20\,°C$ until use. Before use, RNase H was activated by incubation for 1 h at $37\,°C$ in Tris-HCl/K^+/Mg^{2+} buffer (50 mM Tris-HCl, 50 mM KCl, 3 mM $MgCl_2$, 50 mM DTT at pH 8.0.

Oligonucleotides: HPLC-purified lyophilized DNA and RNA oligonucleotides were purchased from Biosearch Technologies (Risskov, Denmark), Metabion International AG (Planegg, Germany) and employed without further purifications. The DNA oligonucleotides were dissolved in phosphate buffer 50 mM, pH 7.0 and stored at $-20\,°C$ until use. The RNA oligonucleotides were dissolved in DEPC-treated water and stored at $-20\,°C$. All the sequences of the different DNA-polymers are reported in the Supporting Information.

DNA-based polymer assembly and reorganization: The DNA tiles for all the systems were prepared as reported elsewhere.[34–35] Tile-forming strands were mixed at 5 μM (final concentration) in aqueous solution containing Mg^{2+} (12.4 mM $MgCl_2$). The solution was annealed with a Bio-Rad Mastercycler Gradient thermocycler by increasing the temperature to $90\,°C$ and cooling it to $20\,°C$ (at a constant rate of $1\,°C/5$ min). The concentrations and buffer conditions employed in the reorganization experiments are reported in the legend of each figure. Detailed procedures of the different fuel-driven reorganization experiments using redox and enzymatic reactions are reported in the Supporting Information.

Confocal laser scanning Microscopy: DNA polymeric structures were imaged using a confocal laser scanning microscope Olympus FV-1000. The emitted photons were collected by a 60x, oil objective. DNA polymeric structures labeled with a different fluorophore (Cy3 and Cy5, see Supporting Information for more details on tile sequences) were imaged using two lasers with different wavelengths (Laser 543 HeNe $\lambda_{ex} = 543$ nm, $\lambda_{em} = 572$ nm; Laser 635 Diodo $\lambda_{ex} = 635$ nm, $\lambda_{em} = 668$ nm).

Fluorescence microscopy: DNA polymeric structures were imaged using an Axio Scope A1 ZEISS microscope. The emitted photons were collected by a 100x oil objective and a monochrome CCD camera (Axiocam 503 mono – ZEISS). Labeled DNA polymeric structures (Cy3 and Cy5, see Supporting Information for more details on tile sequences) were imaged using a Cy3 filter set (EX: 530–550 nm; BS: 565 nm; EM: 575–635) and Cy5 filter set (EX: 590–650 nm; BS: 660 nm; EM: 670–730). Exposure time was set to 10000 ms. Fluorescence microscopy images were processed using ZEN 2 lite (ZEISS) software.

Microscopy data processing: Confocal and fluorescence microscopy images were processed using SPIP Software – Scanning Probe Image Processor – by Image Metrology/Digital Surf (www.imagemet.com) to analyze the number of assembled tiles, average length and pixel intensity profiles of DNA structure collected. Branched structures, aggregates, and structure lengths less than 1 μm were removed from the dataset analysis using SPIP threshold parameters. The colocalization analysis were obtained using Colocalization plugin ImageJ software[39] (see Supporting Information for more details on the calculation of colocalized assembled red and green tiles).

Acknowledgements

Conflict of Interest

The authors declare no conflict of interest.

Data Availability Statement

The data that support the findings of this study are available from the corresponding author upon reasonable request.

[1] J.-M. Lehn, *Science* **2002**, *295*, 2400–2403.
[2] T. Aida, E. W. Meijer, S. I. Stupp, *Science* **2012**, *335*, 813–817.
[3] J. F. Lutz, J. M. Lehn, E. W. Meijer, K. Matyjaszewski, *Nat. Rev. Mater.* **2016**, *1*, 16024.
[4] T. F. A. de Greef, E. W. Meijer, *Nature* **2008**, *453*, 171–173.
[5] P. Besenius, *J. Polym. Sci. Part A* **2017**, *55*, 34–78.
[6] B. Adelizzi, N. J. Van Zee, L. N. J. de Windt, A. R. A. Palmans, E. W. Meijer, *J. Am. Chem. Soc.* **2019**, *141(15)*, 6110–6121.
[7] L. Albertazzi, N. van der Veeken, M. B. Baker, A. R. A. Palmans, E. W. Meijer, *Chem. Commun.* **2015**, *51*, 16166–16168.
[8] A. Sarkar, R. Sasmal, C. Empereur-Mot, D. Bochicchio, S. V. K. Kompella, K. Sharma, S. Dhiman, B. Sundaram, S. S. Agasti, G. M. Pavan, S. J. George, *J. Am. Chem. Soc.* **2020**, *142*, 7606–7617.
[9] O. J. G. M. Goor, S. I. S. Hendrikse, P. Y. W. Dankers, E. W. Meijer, *Chem. Soc. Rev.* **2017**, *46*, 6621–6637.
[10] A. Sarkar, R. Sasmal, A. Das, S. S. Agasti, S. J. George, *Chem. Commun.* **2021**, *57*, 3937–3940.
[11] L. Albertazzi, F. J. Martinez-Veracoechea, C. M. A. Leenders, I. K. Voets, D. Frenkel, E. W. Meijer, *Proc. Natl. Acad. Sci. USA* **2013**, *30*, 12203–12208.
[12] J. B. Gilroy, T. Gädt, G. R. Whittell, L. Chabanne, J. M. Mitchels, R. M. Richardson, M. A. Winnik, I. Manners, *Nat. Chem.* **2010**, *7*, 566–570.
[13] Z. M. Hudson, C. E. Boott, M. E. Robinson, P. A. Rupar, M. A. Winnik, I. Manners, *Nat. Chem.* **2014**, *6*, 893–898.
[14] a) S. Sarkar, A. Sarkar, S. J. George, *Angew. Chem. Int. Ed.* **2020**, *59*, 19841–19845; *Angew. Chem.* **2020**, *132*, 20013–20017; b) A. Sarkar, R. Sasmal, A. Das, A. Venugopal, S. S. Agasti, S. J. George, *Angew. Chem. Int. Ed.* **2021**, *133*, 18357–1836.
[15] D. van der Zwaag, T. F. A. de Greef, E. W. Meijer, *Angew. Chem. Int. Ed.* **2015**, *54*, 8334–8336; *Angew. Chem.* **2015**, *127*, 8452–8454.
[16] R. D. Mukhopadhyay, A. Ajayaghosh, *Science* **2015**, *349*, 241–242.
[17] A. Sorrenti, J. Leira-Iglesias, A. J. Markvoort, T. F. A. de Greef, T. M. Hermans, *Chem. Soc. Rev.* **2017**, *46*, 5476–5490.
[18] A. Jain, S. Dhiman, A. Dhayani, P. K. Vemula, S. J. George, *Nat. Commun.* **2019**, *10*, 450.
[19] a) J. Deng, A. Walther, *J. Am. Chem. Soc.* **2020**, *142*, 685–689; b) J. Deng, A. Walther, *Adv. Mater.* **2020**, *32*, e2002629.
[20] E. Del Grosso, P. Irmisch, S. Gentile, L. J. Prins, R. Seidel, F. Ricci, *Angew. Chem. Int. Ed.* **2022**, *61*, e202201929.
[21] J. Boekhoven, W. E. Hendriksen, G. J. M. Koper, R. Eelkema, J. H. Van Esch, *Science* **2015**, *349*, 1075–1079.
[22] S. Gentile, E. Del Grosso, L. J. Prins, F. Ricci, *Angew. Chem. Int. Ed.* **2021**, *60*, 12911–12917; *Angew. Chem.* **2021**, *133*, 13021–13027.
[23] E. Del Grosso, L. J. Prins, F. Ricci, *Angew. Chem. Int. Ed.* **2020**, *59*, 13238–13245; *Angew. Chem.* **2020**, *132*, 13340–13347.
[24] M. Sun, J. Deng, A. Walther, *Angew. Chem. Int. Ed.* **2020**, *59*, 18161–18165; *Angew. Chem.* **2020**, *132*, 18318–18322.
[25] F. J. Rizzuto, C. M. Platnich, X. Luo, Y. Shen, M. D. Dore, C. Lachance-Brais, A. Guarné, G. Cosa, H. F. Sleiman, *Nat. Chem.* **2021**, *13*, 843–849.
[26] L. N. Green, H. K. K. Subramanian, V. Mardanlou, J. Kim, R. F. Hariadi, E. Franco, *Nat. Chem.* **2019**, *11*, 510–520.
[27] S. Agarwal, E. Franco, *J. Am. Chem. Soc.* **2019**, *141*, 7831–7841.
[28] a) J. Deng, A. Walther, *Nat. Commun.* **2021**, *12*, 1–12; b) J. Deng, W. Liu, M. Sun, A. Walther, *Angew. Chem. Int. Ed.* **2022**, *61*, e202113477.
[29] E. Del Grosso, A. Amodio, G. Ragazzon, L. J. Prins, F. Ricci, *Angew. Chem. Int. Ed.* **2018**, *57*, 10489–10493; *Angew. Chem.* **2018**, *130*, 10649–10653.
[30] E. Del Grosso, G. Ragazzon, L. J. Prins, F. Ricci, *Angew. Chem. Int. Ed.* **2019**, *58*, 5582–5586; *Angew. Chem.* **2019**, *131*, 5638–5642.
[31] S. Gentile, E. Del Grosso, P. E. Pungchai, E. Franco, L. J. Prins, F. Ricci, *J. Am. Chem. Soc.* **2021**, *143*, 20296–20301.
[32] T. J. Fu, N. C. Seeman, *Biochem.* **1993**, *32*, 3211–3220.
[33] A. Ekani-Nkodo, A. Kumar, D. K. Fygenson, *Phys. Rev. Lett.* **2004**, *93*, 268301.
[34] P. W. Rothemund, A. Ekani-Nkodo, N. Papadakis, A. Kumar, D. K. Fygenson, E. Winfree, *J. Am. Chem. Soc.* **2004**, *126*, 16344–16352.
[35] D. Y. Zhang, R. F. Hariadi, H. M. T. Choi, E. Winfree, *Nat. Commun.* **2013**, *4*, 1965.
[36] L. N. Green, A. Amodio, H. K. K. Subramanian, F. Ricci, E. Franco, *Nano Lett.* **2017**, *17*, 7283–7288.
[37] E. Del Grosso, I. Ponzo, G. Ragazzon, L. J. Prins, F. Ricci, *Angew. Chem. Int. Ed.* **2020**, *59*, 21058–21063; *Angew. Chem.* **2020**, *132*, 21244–21249.
[38] E. M. M. Manders, F. J. Verbeek, J. A. Aten, *J. Microsc.* **1993**, *169*, 375–382.
[39] S. Bolte, F. P. Cordelieres, *J. Microsc.* **2006**, *224*, 213–232.
[40] M. Tessier, A. Fradet, *e-Polym.* **2013**, *3*, 30.
[41] P. Nagy, *Antioxid. Redox Signaling* **2013**, *18*, 1623–1641.

[42] E. Del Grosso, E. Franco, L. J. Prins, F. Ricci, *Nat. Chem.* **2022**, *14*, 600–613.

[43] X. Liu, Y. Zhao, P. Liu, L. Wang, J. Lin, C. Fan, *Angew. Chem. Int. Ed.* **2019**, *58*, 8996–9011; *Angew. Chem.* **2019**, *131*, 9092–9108.

[44] H. Pei, X. Zuo, D. Zhu, Q. Huang, C. Fan, *Acc. Chem. Res.* **2014**, *47*, 550–559.

[45] V. J. Schuller, S. Heidegger, N. Sandholzer, P. C. Nickels, N. A. Suhartha, S. Endres, C. Bourquin, T. Liedl, *ACS Nano* **2011**, *5*, 9696–9792.

[46] P. Wang, T. A. Meyer, V. Pan, P. K. Dutta, Y. Ke, *Chem.* **2017**, *2*, 359–382.

[47] C. Sigl, E. M. Willner, W. Engelen, J. A. Kretzmann, K. Sachenbacher, A. Liedl, F. Kolbe, F. Wilsch, S. A. Aghvami, U. Protzer, M. Hagan, S. Fraden, H. Dietz, *Nat. Mater.* **2021**, *20*, 1281–1289.

[48] P. Wang, M. A. Rahman, Z. Zhao, K. Weiss, C. Zhang, Z. Chen, S. J. Hurwitz, Z. Chen, D. M. Shin, Y. Ke, *J. Am. Chem. Soc.* **2018**, *140*, 2478–2484.

[49] B. Saccà, R. Meyer, M. Erkelenz, K. Kiko, A. Arndt, H. Schroeder, K. S. Rabe, C. M. Niemeyer, *Angew. Chem. Int. Ed.* **2010**, *49*, 9378–9383; *Angew. Chem.* **2010**, *122*, 9568–9573.

[50] W. Engelen, C. Sigl, K. Kadletz, E. M. Willner, H. Dietz, *J. Am. Chem. Soc.* **2021**, *143*, 21630–21636.

[51] I. Seitz, H. Ijäs, V. Linko, M. A. Kostiainen, *ACS Appl. Mater. Interfaces* **2022**, *34*, 38515–38524.